

Probing the absorbing haloes around two high-redshift radio galaxies with VLT-UVES^{*}

M.J. Jarvis^{1†}, R.J. Wilman¹, H.J.A. Röttgering¹ and L. Binette²

¹*Sterrewacht Leiden, Postbus 9513, 2300 RA Leiden, The Netherlands.*

²*Instituto de Astronomía, UNAM, Ap.70-264, 04510 México, DF, México.*

2 December 2024

ABSTRACT

We present VLT-UVES echelle spectroscopy of the H I and C IV absorption in the spatially-extended Ly α emission around two high-redshift radio galaxies 0200+015 ($z=2.23$) and 0943-242 ($z=2.92$).

The absorbers in 0943-242 exhibit little additional structure compared with previous low-resolution spectroscopy and the main absorber is still consistent with H I column density of $\sim 10^{19} \text{ cm}^{-2}$. This is consistent with a picture in which the absorbing gas has low density and low metallicity and is distributed in a smooth absorbing shell located beyond the emission-line gas. However, the main absorbers in 0200+015 are very different. The previous single absorber fit of H I column density $\simeq 10^{19} \text{ cm}^{-2}$, now splits into two $\sim 4 \times 10^{14} \text{ cm}^{-2}$ absorbers which extend more than 15 kpc to obscure additional Ly α emission coincident with a radio lobe in these high-resolution observations. Although consistent with the shell-like distribution for the absorption systems, 0200+015 requires a much higher metal enrichment than 0943-242. The metallicity, inferred from the C IV absorption, is considerably lower in 0943-242 than in 0200+015. We explain these differences with an evolutionary scenario based on the size of the radio source. In both sources the H I absorption gas originates from either a gas-rich merger or pristine cluster gas which cools and collapses towards the centre of the dark matter halo. The higher metallicity in the larger radio source (0200+015) may be a result of a starburst driven superwind (concurrent with the triggering of the radio emission) which has engulfed the outer halo in this older source.

We also find a significant blue asymmetry in the He II $\lambda 1640$ emission line, suggesting that the line emitting gas is outflowing from the central regions. Dust obscuration toward the central engine, presumably due to the dusty torus invoked in Unified Scheme, prevents us from seeing outflow away from our line-of-sight.

Key words: galaxies: active - galaxies: halos - galaxies: high-redshift - galaxies: emission lines - galaxies - absorption lines

1 INTRODUCTION

The existence of powerful radio galaxies at high redshift ($z > 2$) demonstrates that a population of supermassive black holes ($> 10^9 M_{\odot}$; Dunlop et al. 2002) was in place just a few billion years after the Big Bang. Like their counterparts at low redshift, the high-redshift radio galaxies (HzRGs) appear to reside in the most massive elliptical galaxies at their epoch (e.g. Jarvis et al. 2001b), in line with the established correlation between black hole and spheroid mass (Magorrian et al. 1998). Whilst the discovery of radio quiet galaxies at high redshift via Lyman drop-out techniques

means that they are no longer our only probe of high redshift galaxy formation, the HzRGs still provide the most important insights into the early formation of the most massive bound structures. Indeed, the depth of the gravitational potential wells in which they form renders them prime targets for searching for high-redshift proto-clusters, as confirmed by the recent discoveries of over-densities of Ly α emitters around such objects (see e.g. Kurk et al. 2000; Pentericci et al. 2000; Venemans et al. 2002).

One of the most prominent characteristics of HzRGs are their extended emission line regions (EELRs), which are luminous ($> 10^{37} \text{ W}$ in Ly α), tens to several hundred kpc in size (often aligned with the radio axis) and kinematically active ($\text{FWHM} \gtrsim 1000 \text{ km s}^{-1}$). Their dominant ionisation mechanism seems to change from shocks to photoionisation by the central engine as the radio source expands beyond the confines of the host galaxy

^{*} Based on observations performed at the European Southern Observatory, Chile (Programme ID: 68.B-0086(A))

[†] Email: jarvis@strw.leidenuniv.nl

(Best et al. 2000; De Breuck et al. 2000; Jarvis et al. 2001a). Likewise the kinematics of the gas may reflect the competing influences of gravity, and energy input via shocks from the radio source and starburst-driven superwinds. However, there are many unresolved issues which remain concerning the structure, origin and fate of the emission line gas, which may hold important clues to many aspects of massive galaxy formation. Did the gas originate in a cooling flow or a merger, or was it expelled from the central galaxy during a violent starburst? Is it in the form of cloudlets, filaments or expanding shells of material, and what is their composition? What is the ultimate fate of the gas, will it form stars or escape from the galaxy to enrich the surrounding intracluster and intergalactic media?

A new perspective on many of these issues was opened up with the discovery by Röttgering et al. (1995) and van Ojik et al. (1997; hereafter vO97) that most of the smaller high redshift radio sources (those with projected linear size $D < 50$ kpc) exhibit spatially resolved HI absorption in their Ly α emission-line profiles, with column densities in the range 10^{18} – $10^{19.5}$ cm $^{-2}$. Binette et al. (2000; hereafter B00) found, for the $z = 2.92$ radio galaxy 0943–242, C IV $\lambda\lambda 1548, 1551$ absorption lines superimposed on the C IV emission, at the same redshift as the main Ly α absorption system. They could not reconcile the observed C IV/Ly α emission- and absorption-line ratios with a model in which the absorption- and emission-line gas are co-spatial. Instead they proposed that the absorbing gas is of lower metallicity ($Z \sim 0.01Z_{\odot}$) and located further away from the host galaxy than the emission line gas, beyond the high pressure radio source cocoon. This material, they claimed, is thus a relic reservoir of low metallicity, low density ($\sim 10^{-2.5}$ cm $^{-3}$) gas, similar to that from which the parent galaxy may have formed. This shell-like distribution of the absorbing gas was also invoked by Jarvis et al. (2001a) and De Breuck et al. (2000) to explain various correlations found in a complete sample of high-redshift ($z > 2$) radio galaxies.

In this paper we probe the HI and C IV absorbers in greater detail using the UVES spectrograph on the VLT to obtain echelle spectra of two high-redshift radio galaxies, the aforementioned 0943–242 and 0200+015 at $z=2.23$. The new observations offer a factor of 10 improvement in spectral resolution over previous investigations and thus have the potential (i) to reveal whether the main absorbers are genuinely in the form of a single component with ordered global kinematics, or whether they fragment into a number of weaker absorbers; (ii) to probe the emission-line kinematics with high velocity resolution.

In section 2 we describe the observations and data reduction of our VLT-UVES spectroscopic observations and in section 3 we briefly discuss the emission- and absorption-line fitting procedure. In section 4 we use our new high-resolution spectra to investigate the absorption halo of the $z = 2.92$ radio galaxy 0943–242. Section 5 is a detailed discussion of the absorbing halo around the $z = 2.23$ radio galaxy 0200+015 and we also investigate the kinematics of the narrow-emission lines via the unabsorbed HeII emission line and briefly discuss the effect of emission-line asymmetry on our absorption line fitting. The origin and fate of the absorbing halos is discussed in section 6 and we provide a summary of our conclusions in section 7.

All physical distances are calculated assuming $H_0 = 70$ km s $^{-1}$ Mpc $^{-1}$, $\Omega_M = 0.3$ and $\Omega_{\Lambda} = 0.7$.

2 OBSERVATIONS AND DATA REDUCTION

The observations were performed with the UVES echelle spectrograph on VLT UT2 at the European Southern Observatory on the night of 2001 December 8–9. For 0200+015, dichroic 1 was used with cross-disperser 1 in the blue arm (central wavelength of 3950 Å, for Ly α), and cross-disperser 3 in the red arm (central wavelength of 5800 Å, for C IV $\lambda\lambda 1548, 1551$ and HeII $\lambda 1640$); three separate exposures of 1 hour were taken. For the 0943–242, just the red arm was used, with cross-disperser 3 set to a central wavelength of 5200 Å, sufficient to cover both Ly α and C IV $\lambda\lambda 1548, 1551$. Separate exposures totalling 3.4 hours were acquired. For all observations on-chip binning of 2×3 (spatial \times spectral) was used, resulting in a pixel size of 0.5 arcsec in the red arm, and 0.36 arcsec in the blue. The resulting pixel scales in the dispersion direction for the various set-ups were in the range 0.05–0.06 Å. Together with a slit-width of 1.2 arcsec, the resulting spectral resolutions were 25000–40000. The seeing was steady throughout the night at ~ 0.8 arcsec, and the sky dark and photometric. The slit position angles were chosen to align with the radio axes and previous observations, namely 155 degrees for 0200+015 and 74 degrees east of north for 0200+015 and 0943–242 respectively.

Offline reduction was performed with IRAF, following the procedures for echelle data described by Churchill (1995). For each target, the individual exposures were median combined to remove cosmic rays, bias-subtracted and flat-fielded. The order-definition frames were used to determine the locations of the orders, which were then extracted and wavelength calibrated using a ThAr arc and combined. The blaze function of the grating was removed using observations of the G-type spectrophotometric standard LTT 1020. Spectra for individual spatial regions along the slit were extracted, rebinned by a factor of 2 in dispersion to improve the signal-to-noise ratio.

3 ANALYSIS

The extracted 1-d spectra were fitted with a series of Voigt absorption line profiles superimposed upon a Gaussian emission envelope. We choose an underlying Gaussian emission-line profile as studies of narrow-line profiles in Seyfert-2 galaxies show that this is preferred over a Lorentzian profile in the majority of cases (e.g. Véron-Cetty, Véron & Gonçalves 2001), but see section 5.2 for further discussion of this point. The model profiles were convolved with the instrumental function prior to fitting (as described by Röttgering et al. 1995 and B00). There is no detected continuum underlying the emission lines.

4 0943–242: CONCLUSIVE EVIDENCE FOR A DISTINCT SHELL OF ABSORPTION-LINE GAS?

Fig. 1 shows the 1-d spectrum of the Ly α and C IV emission lines in 0943–242, extracted over the central 5 arcsec of the slit which covers all of the emission. The fit, with a series of Voigt profile absorbers superimposed upon a Gaussian emission envelope is shown, and the parameters tabulated in Table 1. The errors were calculated by assuming a χ^2 distribution of $\Delta\chi^2$ ($\equiv \chi^2 - \chi^2_{\min}$) (Lampton, Margon & Bowyer 1976). The error on each parameter was calculated by setting $\Delta\chi^2 = 1$ and allowing the other parameters to float. The errors quoted are 1σ .

The most notable feature of this spectrum is that the main absorber remains as a single system of column density $\sim 10^{19}$ cm $^{-2}$,

Absorber	z	b (km s^{-1})	$\log N(\text{HI})$ (cm^{-2})
1	2.9066 ± 0.0062	88 ± 45	14.02 ± 0.30
2	2.9185 ± 0.0001	58 ± 3	19.08 ± 0.06
3	2.9261 ± 0.0005	109 ± 35	13.55 ± 0.16
4	2.9324 ± 0.0001	23 ± 17	13.35 ± 0.30
<hr/>			
			$\log N(\text{CIV})$ (cm^{-2})
2	2.9192 ± 0.0001	119 ± 2	14.58 ± 0.04

Table 1. Parameters of the Voigt absorption profile fits for the main component of 0943-242. The final row corresponds to the fit of one absorber to the CIV profile.

and is completely black at its base with no evidence for substructure. No new absorption systems are identified in addition to those found by Röttgering et al. (1995) at a factor of ~ 10 lower resolution.

This provides strong evidence that these absorption systems are physically distinct from the extended narrow-emission-line region. If the absorption was caused by gas which is mixed with the emission-line clouds, as postulated by vO97 then we would expect a series of narrow-absorption troughs at various wavelengths across the $\text{Ly}\alpha$ emission profile. The fact that we see one main absorber, with no detectable substructure, shifted blueward of the emission-line peak provides compelling evidence that the absorption gas encompasses the whole of the emission-line regions with a covering factor of unity along our line-of-sight. This is in line with the argument proposed by B00 who fitted the emission- and absorption-line profile of the $\text{CIV}\lambda\lambda 1548, 1551$ doublet in 0943-242 to determine the metallicity of the absorption systems compared to the emission-line gas. Their results show that the emission and absorption line ratios of CIV and $\text{Ly}\alpha$ are incompatible with photoionisation or collisional ionisation of cloudlets with uniform properties and the possibility that the absorption and emission phases are co-spatial is rejected. A different model was preferred in which the absorption gas has low metallicity and is located further away from the host galaxy than the emission line gas.

5 0200+015: A DETAILED STUDY

In this section we provide an in depth study of the absorption systems around the $z = 2.23$ radio galaxy 0200+015. This object was taken from the original sample of vO97 and was chosen on account of its interesting absorption-line profile in the $\sim 2\text{\AA}$ resolution spectrum of vO97. A further advantage of using this object for our study is that its redshift permits further observations of all of the principal optical emission lines in the near-infrared transmission windows arising from AGN phenomena which will enable us to determine line ratios and investigate the ionisation mechanisms at work as a function of radial distance from the central source.

Examination of the $\text{Ly}\alpha$ region of the CCD frame of this object shows that the emission deviates from the centre of the order (as defined by the order definition frame) as a function of wavelength. This reflects spatial extent in the emitting and absorbing gas. Spectra were extracted for 2 spatial regions: the main body of the galaxy between ± 1.25 arcsec of the centroid, and a secondary component lying between 1.25–2.5 arcsec to the north-west (1 arcsec translates into 8 kpc at this redshift), coincident with one of

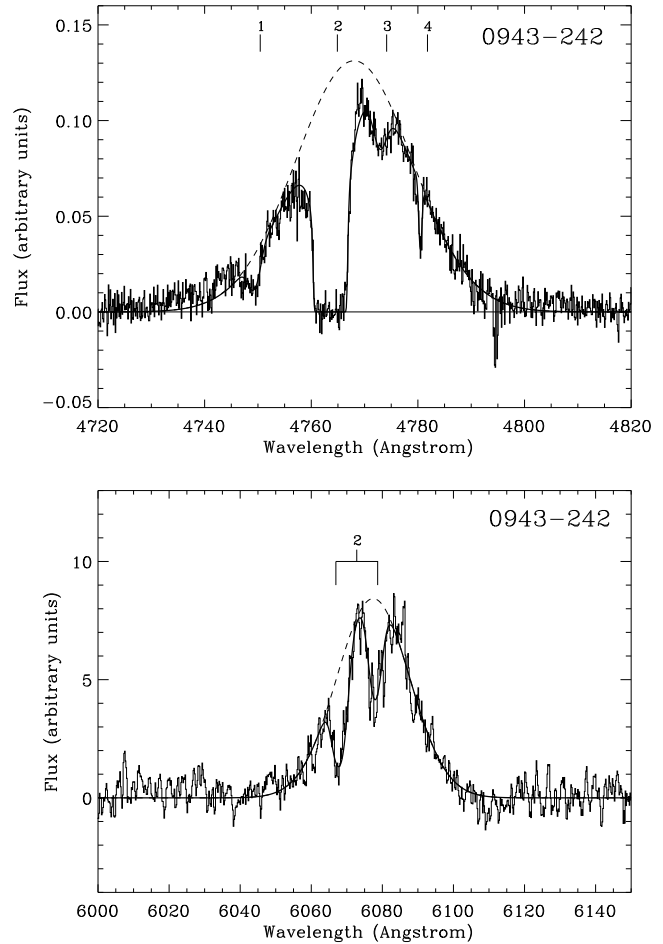


Figure 1. (top) The $\text{Ly}\alpha$ profile of 0943-242, with the absorption model overlaid. (bottom) The CIV profile of 0943-242, with the absorption model overlaid.

Table 2. Parameters of the Voigt absorption profile fits for the main component of 0200+015

Absorber	z	b (km s^{-1})	$\log N(\text{HI})$ (cm^{-2})
1	2.2239 ± 0.0007	612 ± 70	14.96 ± 0.06
2	2.2282 ± 0.0002	116 ± 27	14.73 ± 0.14
3	2.2307 ± 0.0001	61 ± 8	14.58 ± 0.16
4	2.2349 ± 0.0001	86 ± 11	14.38 ± 0.10

the two radio lobes (see the radio continuum image in Carilli et al. 1997). Spectra with overlaid absorption models for these two components are shown in Fig. 2, and the parameters tabulated in Tables 2 and 5.

5.1 The $\text{Ly}\alpha$ emission from the nucleus

The core $\text{Ly}\alpha$ emission-line profile (i.e. the emission associated with the centre of the radio galaxy host) has a redshift of $z = 2.2292$ and full width half maximum $\text{FWHM} = 1490 \text{ km s}^{-1}$. The emission line exhibits a number of absorbers within 320 km s^{-1} of the redshift of the peak of the $\text{Ly}\alpha$ emission, consistent with the lower resolution spectrum of vO97. However,

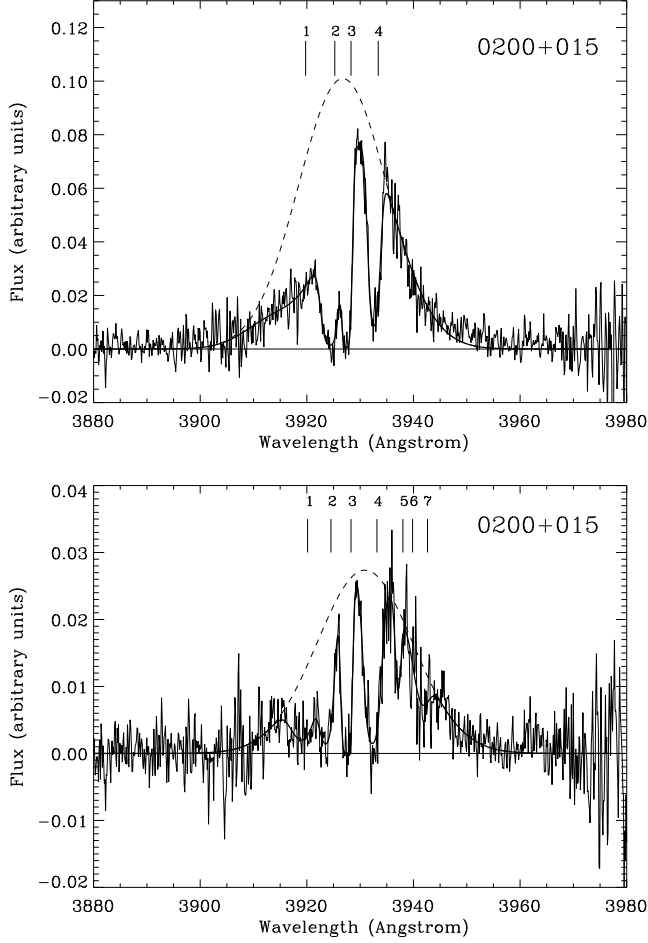


Figure 2. (a) (*top*) The Ly α profile of the central 2.5 arcsec of 0200+015, with the Gaussian emission envelope and the absorption model overlaid. (b) (*bottom*) As in (a) but for the secondary (offset) component of 0200+015, with the absorption model overlaid.

at this higher resolution we do find that the main absorber, with a measured column density of $N_{\text{HI}} = 10^{19.1} \text{ cm}^{-2}$ from vO97, is actually comprised of two absorption troughs with column densities of $N_{\text{HI}} = 10^{14.73} \text{ cm}^{-2}$ and $N_{\text{HI}} = 10^{14.58} \text{ cm}^{-2}$ with velocity widths of 116 km s^{-1} and 61 km s^{-1} and redshifts of $z = 2.2282$ and $z = 2.2307$ respectively.

There is also a $N_{\text{HI}} = 10^{15} \text{ cm}^{-2}$ absorber blueward of these lines if our Gaussian emission profile is accurate. This absorption trough has a much higher Doppler parameter of $b = 612 \text{ km s}^{-1}$, although the sensitivity of this absorption profile on the fit to the emission line is significant and we explore this further in section 5.2.

5.2 Emission-line asymmetry and the evidence for outflow

One of the very noticeable aspects of the spectroscopic data on these two high-redshift radio galaxies is that in the HeII emission line, in which associated absorption does not affect the profile of the emission line, the blue side of the emission line has a longer tale than the redward side (Fig. 3). Using the profile analysis originally defined by Heckman et al. (1981) we assign a relative asymmetry, AI, to the emission at varying fractions of the total intensity where $\text{AI} = 2[\Lambda_c - \lambda_c(i)]/\omega(i)$. Here $\lambda_c(i)$ and $\omega(i)$ are the

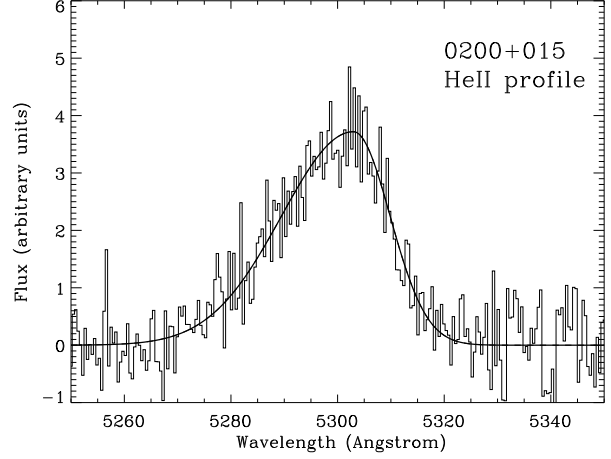


Figure 3. The HeII profile of the central 2.5 arcsec of 0200+015.

Table 3. Asymmetry of the HeII line in 0200+015

per cent of peak (<i>i</i>)	$\lambda_c / \text{\AA}$	$\omega / \text{\AA}$	AI
10	5296.4	43.6	29.4
20	5296.9	36.1	32.4
33	5298.1	29.9	31.8
50	5298.9	23.0	33.9

line centre and width at relative intensity *i*, respectively, and Λ_c is the wavelength of the peak of the profile. The results of the profile analysis are presented in Table 4. Using the FWHM of the asymmetric profile to determine the velocity dispersion of this line we find $v \approx 1920 \text{ km s}^{-1}$.

This blue-tail line asymmetry has been found previously for the narrow-line regions in many Seyfert galaxies (e.g. De Robertis & Shaw 1990) and is probably associated with an inflow or outflow of the gas into or from the central regions. Evidence from narrow-line Seyfert galaxies points towards the view that the asymmetry is caused by outflowing gas propagating towards us along our line-of-sight. The counter flow, which would produce a red-tail asymmetry, is obscured by dust residing within the radius of the narrow-emission-line region. This is in line with the dusty torus invoked in orientation based Unified Schemes. The alternative view, that of inflowing gas, requires the dust to be mixed with the emission-line clouds. This would mean that the blue tail emanates from the far side of the galaxy. In this case the illuminated clouds on the near side along our line of sight suffer higher extinction than the illuminated clouds on the far side (e.g. De Robertis & Shaw 1990). However, ISO observations of NGC 4151 show that this explanation is not sufficient to explain the emission-line characteristic in the infrared where the emission lines are much less susceptible to obscuration. Sturm et al. (1999) propose a central, optically thick obscuring screen close to the nucleus with outflowing emission-line regions, most plausibly associated with a nuclear outflow or a starburst.

Obviously, this particular characteristic of the emission line region needs exploring further with high-resolution spectroscopy of emission lines with a range in ionisation parameters to determine whether the velocity of the material is dependent on the density of the gas and its distance from the central ionizing source. However,

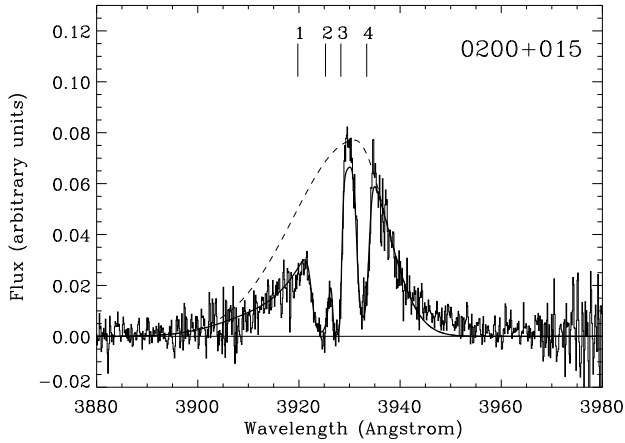


Figure 4. The $\text{Ly}\alpha$ profile of the central 2.5 arcsec of 0200+015 fitted with an asymmetric Gaussian with the same asymmetry as the HeII emission line.

for the purposes of this paper where we are predominantly concerned with the absorbing shells, it highlights the fact that assuming a simple Gaussian profile for the narrow emission lines may be too simple. We have therefore refitted the $\text{Ly}\alpha$ and C IV emission lines for our two objects to determine whether this amount of asymmetry may significantly affect our fitted parameters to the absorption troughs in any way.

We refitted our emission-line profiles with two single tailed Gaussians with common peak intensities and a fixed ratio of FWHM derived from the asymmetry in the HeII line as a simple approximation to the asymmetry profile. Although we note that the different ionisation potential for $\text{Ly}\alpha$ and C IV compared to HeII may affect the asymmetric profile, we do not expect this to be a significant difference given the uncertainties in our model fitting. With this fixed asymmetry the resulting fits to the absorption troughs in both $\text{Ly}\alpha$ and C IV are not significantly altered, these fitted parameters are listed in Table 3

We therefore conclude that although there is evidence for line asymmetry in the narrow-emission-lines in HzRGs this does not alter the fits to the absorption troughs significantly and the original results are still valid. This is quite surprising given the uncertainties arising from the emission-line profile. However, we note that it is very difficult to change the actual absorption columns given any reasonable $\text{Ly}\alpha$ emission-line profile. This is particularly true where the emission is at a low level, i.e. around absorber #1 in Fig. 2 and Fig. 4. Whereas the largest errors occur near the peak of the emission where the absorbing columns (absorbers #2 and #3) have larger associated errors. Furthermore, the fits to absorbers #2 and #3 are more tightly constrained in b because the higher degree of absorption at lower b means that there is little room to manoeuvre in the absorption line fitting. The combination of these effects results in little variation in the absorptions line column densities. However, we note that more extreme $\text{Ly}\alpha$ emission-line profiles will result in larger errors on the absorption-line fits in the wings of the emission line.

5.3 The $\text{Ly}\alpha$ emission associated with the radio lobe

We also observe relatively bright $\text{Ly}\alpha$ emission at the position of one of the radio lobes associated with 0200+015. This emission lies

Table 4. Parameters of the Voigt absorption profile fits for 0200+015, assuming asymmetric emission-line profile using the asymmetry parameters from the HeII emission line. The top panel is for the four absorbers in the $\text{Ly}\alpha$ emission line from the nucleus, the lower panel represents the single absorber in the C IV profile.

Absorber	Line	z	b (km s^{-1})	$\log N(\text{HI})$ (cm^{-2})
1	$\text{Ly}\alpha$	2.2206 ± 0.0012	874 ± 130	14.93 ± 0.07
2	$\text{Ly}\alpha$	2.2282 ± 0.0003	120 ± 25	14.71 ± 0.12
3	$\text{Ly}\alpha$	2.2307 ± 0.0001	55 ± 7	14.52 ± 0.17
4	$\text{Ly}\alpha$	2.2349 ± 0.0001	83 ± 11	14.39 ± 0.09
<hr/>				
				$\log N(\text{CIV})$ (cm^{-2})
2	C IV	$2.2285 \pm <0.0001$	59 ± 2	14.64 ± 0.01

≈ 2.5 arcsec (≈ 20 kpc) away from the nuclear emission. The best-fit Gaussian profile to this emission line shows that the emission has a slightly higher redshift than that found towards the central radio nucleus ($\delta v \sim 150 \text{ km s}^{-1}$) and has a FWHM = 1580 km s^{-1} .

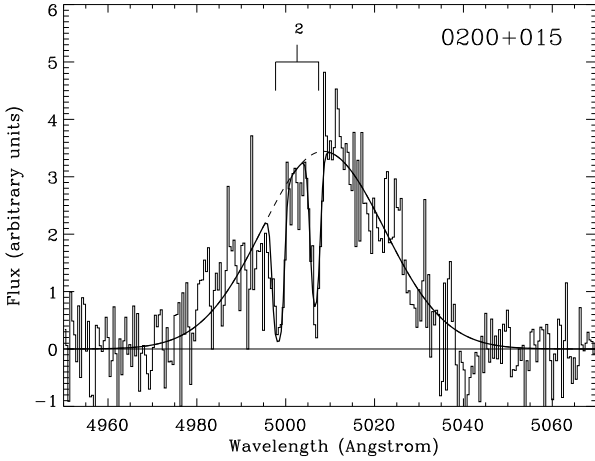
This emission is presumably due to the passage of the radio emitting plasma disrupting the gas at these radii. Invoking the scenario set out by Jarvis et al. (2001a) based on the model of Bremer, Fabian & Crawford (1997), in which the very extended narrow-emission-line regions are compressed and shredded by the radio jets, then this line emission may have been associated with the innermost low-density absorbing shell, which has condensed enough to be seen in emission. This would also explain the slight velocity shift of this emission line if the radio jet, which has essentially boosted this emission, is propagating away from our line-of-sight. However, regardless of the process by which the $\text{Ly}\alpha$ photons are emitted, the surrounding absorbers are distributed in the same way as we see in the nuclear $\text{Ly}\alpha$ emission. This is probably the most compelling evidence that the absorbing gas is distributed in a shell encompassing the whole of the radio galaxy with a covering factor of ≈ 1 , in line with our conclusions for 0943-242. The velocity difference of the absorption systems detected in the $\text{Ly}\alpha$ emission associated with the nuclear emission and that at the position of the lobe is $\sim 30 \text{ km s}^{-1}$, thus we can be quite confident that the absorption systems seen in the lobe emission are associated with the absorption systems associated with the nuclear emission.

We also find more absorbers in this extended emission line in addition to the four main absorbers found in the nuclear $\text{Ly}\alpha$ emission line. These additional absorbers are on the red side of the $\text{Ly}\alpha$ emission line and have significantly lower column densities. The largest velocity offset from the $\text{Ly}\alpha$ emission-line redshift for these redshifted absorption systems is $\sim 600 \text{ km s}^{-1}$. The lower measured column densities of the absorption gas, implies that the covering factor is lower along the line-of-sight to the emission associated with the lobe.

If we assume that the emission from the lobe, which is redshifted with respect to the $\text{Ly}\alpha$ emission-line redshift at the nucleus, is on the far side and is propagating away from us, then any emission from this position would have to pass through both a lower column density redshifted HI component associated with the far side and the bulk of the gas on the near side which is blueshifted. This would explain the higher column density absorbing gas on the blue wing of the emission line.

Table 5. Parameters of the Voigt absorption profile fits for the secondary component of 0200+015

Absorber	z	b (km s^{-1})	$\log N(\text{HI})$ (cm^{-2})
1	2.2241 ± 0.0010	216 ± 110	14.68 ± 0.26
2	2.2276 ± 0.0002	106 ± 29	14.52 ± 0.22
3	2.2307 ± 0.0001	61 ± 11	14.70 ± 0.24
4	2.2347 ± 0.0002	111 ± 21	14.63 ± 0.16
5	2.2387 ± 0.0003	44 ± 37	13.69 ± 0.35
6	2.2402 ± 0.0008	24 ± 22	13.23 ± 0.65
7	2.2423 ± 0.0018	87 ± 59	13.95 ± 0.58

**Figure 5.** The CIV profile of 0200+015, with the vertical ticks indicating the location of the absorption doublet.

5.4 The CIV emission from the nucleus

In the red arm of the spectrum, emission lines of the $\text{CIV}\lambda\lambda 1548\text{\AA}, 1551\text{\AA}$ doublet and $\text{HeII}\lambda 1640\text{\AA}$ are present. The former is shown in Fig. 5, extracted across the entire galaxy because no spatial structure was evident¹ and rebinned in wavelength by a factor of 10 to improve the signal to noise ratio. From our line fitting we find that the centre of the emission line is redshifted with respect to the nuclear $\text{Ly}\alpha$ emission line by $\sim 140 \text{ km s}^{-1}$, however this may be an artifact of trying to fit a symmetric line profile (cf. section 5.2) with a $\text{FWHM} = 1940 \text{ km s}^{-1}$.

A clear absorption doublet can be identified, corresponding to $\text{CIV}\lambda\lambda 1548\text{\AA}, 1551\text{\AA}$ at $z \simeq 2.2285$, i.e. roughly corresponding to absorption system #2 in $\text{Ly}\alpha$ (see Tables 2 and 5). CIV absorption due to $\text{Ly}\alpha$ absorber #3 would appear at $\simeq 5001\text{\AA}, 5010\text{\AA}$ but

¹ Using the $\text{Ly}\alpha$: CIV emission-line flux ratio at the nucleus, our observations are not sensitive enough to detect the expected flux in CIV at the position of the radio lobe.

Table 6. Parameters of the Voigt absorption profile fits for the CIV component of 0200+015.

Absorber	z	b (km s^{-1})	$\log N(\text{CIV})$ (cm^{-2})
2	$2.2285 \pm < 0.0001$	69 ± 1	14.69 ± 0.02

no obvious signature is present. $\text{Ly}\alpha$ absorber #4 would appear at $\simeq 5007\text{\AA}, 5017\text{\AA}$ respectively, thus the 1548\AA trough would overlap on the 1551\AA trough of absorber #2. However, the lack of any apparent absorption at $\sim 5017\text{\AA}$ suggests that the CIV absorption column is significantly lower (and is consistent with no CIV absorption at all) in this shell as compared to that associated with absorber #2, and we assume that all of the CIV absorption can be accounted for by associating it with $\text{Ly}\alpha$ absorber #2. This implies a metallicity gradient in the environment of this radio source. Overzier et al. (2001) recently found strong evidence for a metallicity gradient within the gaseous halo of the $z = 2.49$ radio galaxy MRC2104-242. Overzier et al. (2001) attributed this metallicity gradient to a scenario in which the gas is associated with a massive cooling flow or originates from a merging event. This scenario can also be extended to the absorption gas, and we return to this point in section 6. However, one should keep in mind that the measured N_{CIV} is an upper limit, due to possible extra absorption from the other absorption shells.

5.5 The metallicity of the absorbing shell

In this section we investigate whether the absorption- and emission-line gas can exist co-spatially or whether they are distributed differently based on ionisation models of gaseous slabs with the column densities we observe. We use the method of B00 to investigate the metallicity of the absorbing shell #2 which is the only one clearly seen in absorption in CIV. We use the observable quantity Γ as described by B00 to describe the various ratios between the emission- and the absorption-line properties of both $\text{Ly}\alpha$ and CIV. Γ is defined as

$$\Gamma = \frac{I_{\text{CIV}} N_{\text{HI}}}{I_{\text{Ly}\alpha} N_{\text{CIV}}}, \quad (1)$$

where $I_{\text{CIV}}/I_{\text{Ly}\alpha}$ is the ratio of the emission-line fluxes and $N_{\text{HI}}/N_{\text{CIV}}$ is the ratio of the measured absorption columns. These four quantities carry information on the three ionisation species H^0 , H^+ and C^{+3} .

5.5.1 Co-spatial absorption and emission line gas

Using the current spectra and the Gaussian fit to the emission lines, we obtain $I_{\text{CIV}}/I_{\text{Ly}\alpha} = 0.12 \pm 0.10^2$. Adopting the column of $\text{Ly}\alpha$ absorber #2 in Table 2 and that of CIV in Table 6, we obtain $N_{\text{HI}}/N_{\text{CIV}} = 1.09 \pm 0.04$, hence $\Gamma \approx 0.13 \pm 0.12$. This is a factor of $\sim 5 \times 10^4$ smaller than the value found by B00 for 0943-242 of $\Gamma = 5400$. B00 used the high Γ value in 0943-242 as evidence that the absorbing gas was physically distinct from the emission line regions and was of much lower density and metallicity. Calculations with the MAPPINGS Ic code (Ferruit et al. 1997) indicate that our extremely small value of Γ effectively rules out that the same solar metallicities characterize both the emission- and the absorption-line regions. In fact, reproducing a Γ of 0.13 requires a metallicity of $\sim 10 Z_{\odot}$ if we insist that the absorption and emission gas components have the same metallicities. Therefore, it is theoretically possible to reproduce Γ with a strong overabundance of metals, which may suggest that the emission gas and absorption gas might be more directly inter-related in 0200+015 than in 0943-242. On the other hand, the fact that the emission has such a large FWHM

² The error quoted is the 1σ uncertainty derived from the symmetric and asymmetric Gaussian fits to the emission-lines of both $\text{Ly}\alpha$ and CIV.

as compared to the b values of the absorption profiles and the near unity covering factor of the absorption gas, would still favour the simple picture in which the absorption gas is more quiescent, possibly situated in quasi-uniform shells which are either expanding or infalling.

5.5.2 An absorbing shell surrounding the emission-line region

We now consider the absorption gas in isolation and attempt to explain the process by which the C IV column can be approximately equal to that of H I in the case of absorber #2. At a given metallicity, there exists a physical upper limit to the $N_{\text{CIV}}/N_{\text{HI}}$ column ratio which photoionisation models cannot exceed. This is shown in Fig. 6 which show photoionisation calculations by an ionizing continuum of photon index $\alpha = -1$ ($F_\nu \propto \nu^\alpha$) as a function of the ionisation parameter³ U . The geometry considered was that of an optically thin slab with all models having the same thickness in N_{HI} of $10^{14.73} \text{ cm}^{-2}$. Inspection of Fig. 6 shows that the solar metallicity curve cannot reach the observed value of 0.9 while a slab of $10 Z_\odot$ can again reproduce the target ratio. If the ionisation process, however, was dominated by collisional ionisation, then one could not rule out solar metallicity. This is shown by the dashed-line in Fig. 6 which represents a slab which is initially photoionised with a low value of U but where the temperature is imposed. The temperatures are increasing (starting from the equilibrium value of 13000 K) in steps of 0.1 dex and collisional ionisation progressively takes over. The open squares identify the first eight models, up to $8.2 \times 10^4 \text{ K}$. To show that the column ratio actually decreases at much higher temperatures, we used filled triangles to denote the models in which the temperature starts from $1.03 \times 10^5 \text{ K}$ and increases in steps of 0.1 dex. We have verified that, as expected, the peak reached in the column ratio is not higher for a slab with higher ionisation parameter (the peak is actually lower for $U \geq 0.01$).

We infer from the above calculations that a solar metallicity would therefore require an unusual fine tuning in order to give a temperature which lies in the range of $\sim 0.7\text{--}1.4 \times 10^5 \text{ K}$. This is not a very probable state for any astrophysical plasma since this is exactly the same temperature range across which the cooling curve is known to peak (e.g. Fig. 8 in Ferruit et al. 1997). For the gas to be maintained in this temperature range would require an additional (unknown) heating mechanism. Cooling shocks can in principle reproduce the observed C IV columns but the models so far computed indicate huge N_{HI} columns $\sim 10^{19} \text{ cm}^{-2}$ (see Table 2D in Dopita & Sutherland 1996), a value which is many orders of magnitude beyond the observed value for absorber #2 of $10^{14.73} \text{ cm}^{-2}$. For these reasons, it appears to us more plausible to invoke metal-rich absorbing gas.

Therefore, although the value of Γ in 0200+015 (unlike 0943-242 cf. B00) can be reconciled with a co-spatial distribution of absorption- and emission-line gas, this is not our preferred scenario given the additional information, i.e. the fact that the emission has such a large FWHM as compared to the b values of the absorption profiles and the near unity covering factor of the absorption gas. Therefore, the original conclusions of B00 still hold in which the absorption gas resides in a shell-like distribution, but we are now in a situation where the metallicity and the density of the absorption shells varies from shell-to-shell in the same source and also from source-to-source.

³ $U = \frac{Q}{4\pi r^2 c n}$, where $Q = \int \frac{L_\nu}{h\nu} d\nu$, r is the distance to the cloud from the ionising source and n is the particle density.

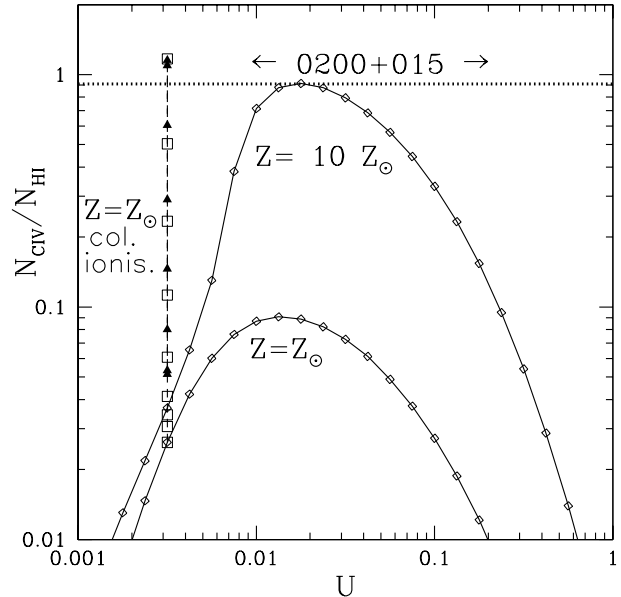


Figure 6. The column ratios $N_{\text{CIV}}/N_{\text{HI}}$ in photoionisation models as a function of the ionisation parameter U (represented by open diamonds joined by a solid line). The lower and upper curves correspond to gas with solar and 10 times solar metallicity, respectively. The dashed-line corresponds to models whose temperature has been increased in steps starting from the equilibrium value of 13000 K (open squares for $T \leq 82000 \text{ K}$, filled triangles at higher T). The $N_{\text{CIV}}/N_{\text{HI}}$ column ratio actually decreases when the temperature exceeds 10^5 K . All models correspond to slabs for which the N_{HI} column is $10^{14.73} \text{ cm}^{-2}$ as in 0200+015 (absorber #2 in Table 2). The dotted horizontal line represents the observed value of $N_{\text{CIV}}/N_{\text{HI}}$ ratio in 0200+015.

6 DISCUSSION

6.1 Origin of the absorbing shells

In this section we speculate on the origin of the large absorption shells around HzRGs.

6.1.1 Shells propagated by the passage of radio jets

The evidence presented in this paper suggests that the absorbing shells surround the whole of the radio source and probably have a roughly spherical distribution. If this is the case then it is extremely unlikely that the shells are propagated by the passage of the radio emission for which we would expect the shells to be disrupted at radii less than the extent of the radio emission. The fact that we see the absorption systems in the majority of the smaller radio galaxies (projected linear size $D < 50 \text{ kpc}$) but not in the larger sources (e.g. van Ojik et al. 1997) makes this scenario very unlikely. We also observe the absorption systems along the line-of-sight to the nucleus. Given that radio galaxies are orientated along the plane of the sky according to orientation based unified schemes, then this also rules out the scenario of a radio jet propagated shell.

6.1.2 Starburst driven superwinds

One explanation is that the shells originate at the centre of the galaxy and are ejected by superwinds, like those seen in Lyman Break galaxies (e.g. Steidel 2001). These winds will propagate

roughly spherically, provide an explanation of the enriched nature of the shells and have no problem in explaining the number of shells and the diverse metallicities if the starburst driven winds are episodic.

Evidence is mounting that powerful radio galaxies are formed at an early epoch and the triggering of the AGN activity is synchronized with a major episode of star formation (e.g. Archibald et al. 2001; Willott et al. 2002; Baker et al. 2002). Therefore, it seems likely that starburst driven superwinds may be an important mechanism for ejecting gas out of the central regions and the high dust concentrations inferred from submillimetre observations imply that starburst may easily be obscured at UV and optical wavelengths.

Martin (1999) and Heckman et al. (2000) estimated the outflow speeds of superwinds for galaxies of varying mass. They show that the outflow speed is largely independent of galaxy mass, implying that the outflows preferentially escape less massive halos. High-redshift radio galaxies seem only to be found in the most massive elliptical galaxies at any redshift (e.g. Jarvis et al. 2001b), hence presumably the deepest potential wells. If this is the case then unlike the case for L^* and sub- L^* galaxies the winds may not possess the required velocity to fully escape the deep potential well and subsequently enrich the intergalactic medium beyond the confines of the HzRG dark halo. Instead this enriched material resides at large radii, away from the central cusp, but still within the potential well of the galaxy.

In the event of episodic superwinds, these shells would eventually collide at large radii, which could both deplete or increase the metallicity of the most distant shell depending on the composition of the wind. If this is the case then these shells will eventually fall back towards the centre of the shell in the absence of a repulsive force. Indeed, with reference to Tables 1 and 2, there is a slight tendency for the $\text{Ly}\alpha$ absorbers in 0200+015 to have lower neutral column densities and b -parameters as the absorption redshift (z_{abs}) increases. If the difference between z_{abs} and the redshift of the emission line peak reflects outflow of the shell relative to the radio galaxy, this trend could reflect evolution in the ionisation state and internal structure of the shells as they are ejected from the radio galaxy.

This is in line with an initial major burst of star formation in which much of the gas is expelled, subsequently followed by smaller bursts in which the lower velocity, lower-density shells are expelled. At some stage in the evolution these shells would fall back under gravity and the shells would merge, but this process is probably very rare because the radio jet has already disrupted the outermost shells which are now seen in emission. However, it is difficult to reconcile the low metallicity shells in 0943-242 with a starburst scenario, as we would expect much higher enrichment if the shells originate in a starburst driven superwind. Although this is not the case for the high metallicity shell in 0200+015.

6.1.3 Relics from a gas-rich merger

Metal enriched shells of low-density gas could be a relic from a gas-rich merger in which there was an episode of star-formation, presumably induced by the merger. This scenario has been used to explain the vast HI shells in low-redshift elliptical galaxies (e.g. Sahu et al. 1996; Morganti et al. 1997).

A number of numerical investigations predict that the outer regions of a galactic halo should be less metal rich than the central regions (e.g. Bekki 1998). This is in line with the case of 0943-242 but in opposition to the case of 0200+015 in which the main

absorber is highly enriched and is comparable in metallicity to that expected in the narrow-emission line region towards the centre.

An argument against the merger relic scenario is that the efficiency of mergers depends critically on the relative velocities, with low velocity mergers being the most efficient. This means that these efficient mergers would produce very low velocity dispersions in the absorbing gas. We might also expect the low density halo resulting from a gas-rich merger to have a more filamentary structure with a covering factor less than unity, which although reconcilable with our observations of a unity covering factor along our line-of-sight, is not the most plausible explanation. Therefore although a gas-rich merger remains a candidate for producing the extended low-metallicity haloes it has difficulties in producing the enriched shell we see in 0200+015 and probably needs a very specific merging scenario.

6.1.4 Gas-rich clusters and cooling flows

It is now well established that many powerful radio galaxies reside in significant galaxies overdensities at all cosmic epochs (e.g. Hill & Lilly 1991; McLure & Dunlop 2001; Best 2001; Pentericci et al. 2000). Indeed, the discovery of $\sim 20 \text{ Ly}\alpha$ emitters around a $z = 4.1$ radio galaxy (Venemans et al. 2002) suggests that powerful radio galaxies are ideal beacons for tracing proto-clusters in the early Universe. If this is ubiquitous for all powerful radio galaxies then we might expect large reservoirs of gas around the radio galaxy.

Within a cluster, cooling flows provide a mechanism for depositing substantial amounts of cool gas and dust around the central galaxy (e.g. Edge 2001). The observational consequences of a radio source being triggered at the centre of such a cooling flow cluster at high redshift were discussed by Bremer et al. (1997). One of their clearest predictions concerns the presence of HI absorption in the $\text{Ly}\alpha$ emission in systems seen as radio galaxies (as opposed to radio-loud quasars): to see absorption from an ensemble of clouds requires a covering fraction of at least 50 per cent; little absorption is expected from clouds at radii of 10–100 kpc, as their covering fraction is low, but those between 10–20 kpc provide a covering fraction of order unity and absorbing HI columns of $10^{18} - 10^{21} \text{ cm}^{-2}$, as the surrounding gas away from the ionising beam should be similar to that of the interstellar medium before the nucleus became active.. This would account for the absorption in 0943-242 where the radio source has a projected linear size $\sim 26 \text{ kpc}$; in 0200+015, however, the radio source is larger ($\sim 43 \text{ kpc}$) and has already engulfed these high-covering factor clouds, so the absorbers in this object may have been disrupted.

However, the classical view of a cooling flow, from low-redshift studies is almost certainly not applicable at these high redshifts. The main reason for this is that the environmental gas may not have had time to both settle towards hydrostatic equilibrium and also to be heated up to X-ray temperatures. In the low-redshift Universe cooling flows also have an inclination to produce filaments when the gas cools (e.g. Fabian et al. 1981), which would result in a much reduced covering factor ($\ll 1$; see e.g. Conselice, Gallagher & Wyse 2001). Therefore, a possibly more accurate view is one in which the pristine gas is collapsing and cooling in a more globally ordered fashion, i.e. as a spherical collapse. In this case the resulting gaseous distribution would be different from that in a low-redshift cooling flow and have the observed high covering factors.

6.2 A scenario: deposition of pristine gas and triggered star formation

An age based scenario, which assumes that both the AGN activity and a major episode of star formation are synchronized, probably due to the collapse and cooling of (proto-)cluster gas (or a gas-rich merger), may explain the differences in the absorption shells of 0200+015 and 0943-242. The projected linear size D , of the radio emission may be used as an age indicator for the radio source (e.g. Blundell, Rawlings & Willott 1999; Baker et al. 2002). In this case 0200+015 ($D \sim 43$ kpc) is significantly older than 0943-242 ($D \sim 15$ kpc). If this is the case then there is much more time for the absorption shells to have evolved in 0200+015. An indication of this comes from the interaction of the radio emitting plasma in the extended component in 0200+015, which looks to be disrupting the absorption shells and subsequently producing additional emission.

If starburst or quasar driven winds precede the passage of the radio activity then a pristine halo at large radii will be enriched by the winds before the radio plasma propagates through the extended regions. Indeed, in an investigation of the metallicity of the broad-line region in quasars, Hamann et al. (2002) compared the UV emission line ratios in a sample of radio-quiet quasars with theoretical models. They found the broad-line region gas was most likely to be of high metallicity ($Z > Z_{\odot}$) and was a consequence of rapid star formation triggered at or before the time of the quasar activity. Ejection of the gas via a quasar or starburst driven outflow would obviously enrich the surrounding halo and thus offer an explanation of the highly enriched nature of absorber #2 in 0200+015.

In the case of 0943-242 any starburst driven wind associated with the activation of the nucleus may not have had time to enrich the outer halo. Thus the explanation of Binette et al. (2000) still holds for this source, in which the shell has a very low-metallicity.

This would also explain the variety of metallicities observed in these shells, as some of the shells will have been enriched, while the winds have not yet reached the others. This naturally fits in with the absorption lines in 0200+015, in which the blueshifted (absorber #2) shell has a high metallicity, whereas absorbers #3 and #4 lie redward of the $\text{Ly}\alpha$ emission line and are probably infalling components from the (proto-)cluster environment, in which there has been little or no star formation to enrich the shells. This is also in line with the work of Overzier et al. (2001) in which the metallicity gradient in the emission-line gas in the gaseous halo surrounding MRC2104-242 may also arise from the same mechanism.

The fate of the shells is uncertain, it is not implausible that shredding by the passage of the radio jet (e.g. Bremer et al. 1997) will work to condense the shells into distinct clouds that may resemble the knots of emission-line gas observed in many larger radio sources. This naturally fits in with correlation between the extent of the emission-line gas and the extent of the radio emission (e.g. Jarvis et al. 2001a), with the radio emitting plasma propagating through the low-density gas which consequently increases the density of this gas resulting in detectable line emission.

6.3 The link to quasars

Using a complete sample of radio-loud quasars from the Molonglo Quasar Catalogue (Kapahi et al. 1998), Baker et al. (2002) used both the Hubble Space Telescope with STIS and ground based telescopes to investigate the associated C IV absorption in two redshift intervals. They found that the absorbing systems in these objects have similar velocities widths and offsets to the two radio galaxies investigated in this paper, the gas is mixed with a large amount of

dust and that the gas and dust dissipate over the lifetime of the radio source. Thus, the main conclusions from this study fit in easily with our results, in line with Unified schemes.

The advantage that radio galaxies hold over quasars is that, according to unified schemes, the radio galaxies are orientated along the plane of the sky and so the deprojection to the true linear size of the radio source is trivial. Therefore, age effects may become more apparent in a large sample of radio galaxies with higher signal-to-noise observations. This should easily be achievable with current instrumentation as we have shown that spectra of resolution of $\sim 2\text{\AA}$ at these redshifts is sufficient to probe the absorption shells to the required detail allowing the integration time to be significantly reduced. Combined with a similar sample of radio-loud quasars, in which the reddening properties may be explored, we should be able to track the evolution of both the absorption- and emission-line gas and the intrinsic dust properties in all radio-loud AGN.

6.4 Further observations

Obviously further observations of the sources studied in the paper will enhance our understanding of the origin and fate of the gas surrounding HzRGs. Indeed, deep spectroscopy around other resonant lines may provide critical information regarding the state of the absorbing shells. The most obvious emission line to use for this study would be the MgII $\lambda\lambda 2795, 2802$ doublet. The absorption equivalent width ratio of C IV/MgII is frequently used to classify quasar absorbers into high or low excitation (e.g. Bergeron et al. 1994) and will also provide further information regarding the metallicity of the gas.

0200+015 is also at a redshift in which the $\text{H}\alpha$ emission line is redshifted into the near-infrared K -band transmission window. As $\text{H}\alpha$ is not a resonant line the true velocity structure of the $\text{Ly}\alpha$ line should be replicated in $\text{H}\alpha$, thus allowing a detailed study of the actual kinematics of the emission-line gas. The $\text{Ly}\alpha/\text{H}\alpha$ ratio is also sensitive to reddening by dust, and if the $\text{Ly}\alpha$ photons escape from the clouds via resonant scattering from HI, the $\text{Ly}\alpha$ line should have significantly broader wings than that of $\text{H}\alpha$.

Finally, spectroscopic observations around various resonant line of a large sample of high-redshift radio galaxies spanning projected linear sizes from $D \sim 1\text{--}2$ kpc up to the classical doubles with $D \gtrsim 100$ kpc are warranted. These will shed further light on the distribution, density and metallicity of gas in the environments of the most massive galaxies at high redshift, and provide clues as to the origin and fate of these large gaseous halos, and may consequently provide important clues to galaxy formation in general and the important role that feedback may play.

7 CONCLUSIONS

We have obtained high-resolution spectra of two high-redshift radio galaxies to determine the structure of the absorption gas which appears to be ubiquitous in small ($D < 50$ kpc) radio sources. The main conclusions of this study can be summarized as follows:

- The higher resolution observations do not uncover significant structure in the absorbers of both $\text{Ly}\alpha$ and C IV in 0943-242, however the $N_{\text{HI}} \sim 10^{19} \text{ cm}^{-2}$ absorber in 0200+015 split into two absorber of $N_{\text{HI}} \sim 4 \times 10^{14} \text{ cm}^{-2}$. The absorption gas present in our two chosen high-redshift radio sources is most likely distributed in shell-like structures which encompass the radio source.

- The metallicity of these absorption shells can vary between sources and also between the shells in the same sources, implying that the shells are enriched by a secondary process.

- We speculate that the most plausible origin of the absorbing shells is two fold. The pristine shells are the relics from a gas-rich merger or (proto-)cluster gas which has cooled and collapsed towards the centre of the dark matter halo. Whereas the enrichment comes at a later stage when the AGN is triggered simultaneously with a major episode of star formation, presumably due to a large inflow of gas into the nucleus. This major burst of star formation initiates starburst driven superwinds which drive the gas toward the outer halo of the galaxy and may explain the very high metallicity of the absorption shells in 0200+015.

- The passage of the radio emitting plasma disrupts and fragments the absorption shells in the larger, and thus older radio sources. Evidence of this is seen in 0200+015, where the absorption screen along our line-of-sight to the radio lobe appears to be more fragmented than the absorbing screen between us and the nuclear emission.

- We have found direct evidence that the narrow-emission lines in high-redshift radio sources may be outflowing from the central regions. This is in agreement with previous studies of the narrow-emission line dynamics in nearby Seyfert galaxies and is in line with orientation based Unified Schemes in which the outflow from the far side of the source is obscured by dust.

ACKNOWLEDGMENTS

We thank the staff at the Paranal Observatory for their excellent support and Sandro D'Odorico for help with the preparation for the UVES observations. RJW thanks Sara Ellison and Sabine Mengel for their assistance with the data reduction. We thank Jaron Kurk for the use of his IDL routine for Voigt profile fitting. MJJ acknowledges the support of the European Community Research and Training Network "The Physics of the Intergalactic Medium". RJW acknowledges support from an EU Marie Curie Fellowship. LB acknowledges support from the CONACyT grant 32139-E. The data presented in this paper were based on observations performed at the European Southern Observatory, Chile (Programme ID: 68.B-0086(A)).

REFERENCES

- Archibald E.N., Dunlop J.S., Hughes D.H., Rawlings S., Eales S.A., Ivison R.J., 2001, MNRAS, 232, 417
- Baker J.C., Hunstead R.W., Athreya R.M., Barthel P.D., de Silva E., Lehnert M.D., Saunders R.D.E., 2002, ApJ, 568, 592
- Bekki K., 1998, ApJ, 504, 50
- Bergeron J., et al., 1994, ApJ, 436, 33
- Best P.N., 2000, MNRAS, 317, 720
- Best P.N., Röttgering H.J.A., Longair M., 2000, MNRAS, 311, 23
- Binette L., Kurk J.D., Villar-Martin M., Röttgering H.J.A., 2000, A&A, 356, 23
- Blundell K.M., Rawlings S., Willott C.J., 1999, AJ, 117, 677
- Bremer M.N., Fabian A.C., Crawford C.S., 1997, MNRAS, 284, 213
- Carilli C.L., Röttgering H.J.A., van Ojik R., Miley G.K., van Breugel W.J.M., 1997, ApJS, 109, 1
- Churchill C.W., 1995, *Introduction to Echelle Data Reduction using IRAF*, University of California, Lick Observatory Technical Report, No. 74
- Conselice C.J., Gallagher J.S., Wyse R.F.G., 2001, AJ, 122, 2281
- De Breuck C., Röttgering H.J.A., Miley G.K., van Breugel W.J.M., Best P., 2000, A&A, 362, 519
- De Robertis M.M., Shaw R.A., 1990, ApJ, 348, 421
- Dopita M.A., Sutherland R.S., 1996, ApJS, 102, 161
- Dunlop J.S., McLure R.J., Kukula M.J., Baum S.A., O'Dea C.P., Hughes D.H., 2002, MNRAS submitted (astro-ph/0108397)
- Edge A.C., Ivison R.J., Smail I.R., Blain A.W., Kneib J.-P., 1999, MNRAS, 306, 599
- Edge A.C., 2001, MNRAS, 328, 762
- Edge A.C., Wilman R.J., Johnstone R.M., Crawford C.S., Fabian A.C., Allen S.W., 2002, MNRAS in press. (astro-ph/0206379)
- Fabian A.C., Nulsen P.E.J., Stewart G.C., Ku W.H.-M., Malin D.F., Mushotzky R.E., 1981, MNRAS, 196, 35
- Ferruit P., Binette L., Sutherland R. S., Pécontal, E. 1997, A&A 322, 73
- Hamann F., Korista K.T., Ferland G.J., Warner C., Baldwin J., 2002, ApJ, 564, 592
- Heckman T.M., Miley G.K., van Breugel W.J.M., Butcher H.R., 1981, ApJ, 147, 403
- Heckman T.M., Lehnert M., Strickland D., Armus L., 2000, ApJS, 129, 493
- Hill G.J., Lilly S.J., 1991, ApJ, 367, 1
- Jarvis M.J., et al., 2001a, MNRAS, 326, 1563
- Jarvis M.J., Rawlings S., Eales S.A., Blundell K.M., Bunker A.J., Croft S.D., McLure R.J., Willott C.J., 2001b, MNRAS, 326, 1585
- Kapahi V.K., Athreya R.M., Subrahmanya C.R., Baker J.C., Hunstead R.W., McCarthy P.J., van Breugel W., 1998, ApJS, 118, 327
- Kurk J.D., et al., 2000, A&A, 358, L1
- Overzier R.A., et al. Röttgering H.J.A., Kurk J.D., De Breuck C., 2001, A&A, 367, L50 (Erratum A&A, 370, L39)
- Lampton M., Margon B., Bowyer S., 1976, ApJ, 208, 177
- Magorrian J., et al., 1998, AJ, 115, 2285
- Martin C.L., 1999, ApJ, 513, 156
- McLure R.J., Dunlop J.S., 2001, MNRAS, 321, 515
- Morganti R., Oosterloo T.A., Tadhunter C.N., van Moorsel G., Killeen N., Wills K.A., 2001, MNRAS, 323, 331
- Pentericci L., et al., 2000, A&A, 361, L25
- Röttgering H.J.A., Hunstead R.W., Miley G.K., van Ojik R., Wieringa M.H., 1995, MNRAS, 277, 389
- Sahu D.K., Pandey S.K., Chakraborty D.K., Kembhavi A., Mohan V., 1996, A&A, 314, 721
- Steidel C.C., 2001, AAS, 198, 5208
- van Ojik R., Röttgering H.J.A., Miley G.K., Hunstead R.W., 1997, A&A, 317, 358
- Sturm E., Alexander T., Lutz D., Sternberg A., Netzer H., Genzel R., 1999, 512, 197
- Venemans B., et al., 2002, ApJ, 569, 11
- Véron-Cetty M.-P., Véron P., Gonçalves A.C., 2001, A&A, 372, 730
- Willott C.J., Rawlings S., Archibald E.N., Dunlop J.S., 2002, MNRAS, 331, 435